batteries

MDPI

Article

Sodium Citrate Electrolyte Additive to Improve Zinc Anode Behavior in Aqueous Zinc-Ion Batteries

Xin Liu [1], Liang Yue [1], Weixu Dong [1], Yifan Qu [1], Xianzhong Sun [2] and Lifeng Chen [1,*]

[1] CAS Key Laboratory of Mechanical Behavior and Design of Materials (LMBD), School of Engineering Science, School of Chemistry and Materials Science, University of Science and Technology of China, Division of Nanomaterials & Chemistry, Hefei National Research Center for Physical Sciences at the Microscale, Hefei 230026, China; liuxinustc@mail.ustc.edu.cn (X.L.); liang_yue@mail.ustc.edu.cn (L.Y.); dwxsa21013030@mail.ustc.edu.cn (W.D.); sa21013019@mail.ustc.edu.cn (Y.Q.)

[2] Institute of Electrical Engineering, Chinese Academy of Sciences, Beijing 100190, China; xzsun@mail.iee.ac.cn

* Correspondence: chenlf@ustc.edu.cn

Abstract: Despite features of cost-effectiveness, high safety, and superior capacity, aqueous zinc-ion batteries (ZIBs) have issues of uncontrolled dendritic cell failure and poor Zn utilization, resulting in inferior cycling reversibility. Herein, the environmentally friendly and naturally abundant sodium citrate (SC) was adopted as a dual-functional additive for $ZnSO_4$-based (ZSO) electrolytes. Owing to the abundant hydrogen-bond donors and hydrogen-bond acceptors of SC, the Zn^{2+}-solvation shell is interrupted to facilitate Zn desolvation, resulting in inhibited corrosion reactions. Additionally, sodium ions (Na^+) from the SC additive with a lower effective reduction potential than that of zinc ions (Zn^{2+}) form an electrostatic shield inhibiting the formation of initial surface protuberances and subsequent Zn dendrite growth. This assists in the Zn three-dimensional (3D) diffusion and deposition, thereby effectively enhancing cycling stability. Specifically, a long cycling lifespan (more than 760 h) of the Zn//Zn symmetric cell is achieved with a 2 M ZSO-1.0 SC electrolyte at a current density of 1 mA cm^{-2}. When coupled with the $NaV_3O_8 \cdot 1.5\ H_2O$ (NVO) cathode, the full battery containing SC additive exhibited a capacity retention rate (40.0%) and a cycling life of 400 cycles at a current density of 1 A g^{-1} compared with that of pure $ZnSO_4$ electrolyte (23.8%). This work provides a protocol for selecting an environmentally friendly and naturally abundant dual-functional electrolyte additive to achieve solvation shell regulation and Zn anode protection for the practical large-scale application of ZIBs.

Keywords: electrolyte additive; sodium citrate; aqueous zinc-ion batteries; Zn anode protection; solvation shell regulation

Citation: Liu, X.; Yue, L.; Dong, W.; Qu, Y.; Sun, X.; Chen, L. Sodium Citrate Electrolyte Additive to Improve Zinc Anode Behavior in Aqueous Zinc-Ion Batteries. *Batteries* **2024**, *10*, 97. https://doi.org/10.3390/batteries10030097

Academic Editor: Dino Tonti

Received: 21 January 2024
Revised: 22 February 2024
Accepted: 5 March 2024
Published: 11 March 2024

1. Introduction

With the grievous air pollution, scarce fossil fuels, and growing energy demand, the development of clean energy that produces no carbon emissions will have far-reaching effects on global climate and environment [1–3]. However, clean energy, such as tidal energy, wind energy, solar energy, and pumped storage, are intermittent, unpredictable, and decentralized due to the effects of terrain and weather and are not universally applicable. Rechargeable batteries, led by lithium-ion batteries, have become important energy storage devices and are widely used in various fields, such as vehicles, electronic products, and emergency power supply systems, owing to their advantages of high energy density, strong controllability, and operability [4,5]. However, the safety and cost issues of lithium-ion batteries necessitate the development of new types of rechargeable and secondary batteries with zinc (Zn) metal, magnesium (Mg) metal, sodium (Na) metal, aluminum (Al) metal, and potassium (K) metal as anode materials [6,7]. Among them, aqueous zinc-ion batteries (ZIBs) are regarded as one of the best candidates. Firstly, part of the advantage comes from Zn metal as an anode due to its high volume capacity (5855 mAh cm^{-3}), low redox

potential (−0.762 V vs. standard hydrogen electrode), rich reserves of Zn, and low cost [8]. Secondly, another part of advantage comes from the aqueous electrolyte, which has natural safety, high ionic conductivity, low cost, and low environmental requirements for battery assembly compared to organic electrolytes [9,10].

Unfortunately, ZIBs still suffer from dendrite growth, the hydrogen evolution reaction (HER), and side reactions on the anode, which hinder the wide adoption of ZIBs [11]. Specifically, in aqueous electrolytes, Zn^{2+} usually forms a stable $[Zn(H_2O)_6]^{2+}$ solvation shell with six water molecules [12]. This stable solvated $[Zn(H_2O)_6]^{2+}$ inhibits Zn^{2+} desolvation and deposition at the electrode–electrolyte interface, which immensely triggers the HER and results in increased OH^- concentration [13]. In the presence of Zn^{2+} and OH^-, byproducts, such as $Zn_4SO_4(OH)_6{\cdot}5H_2O$ (ZSH), are formed in large quantities, which will passivate the Zn anode surface, increase the interface impedance, hinder Zn deposition. More seriously, in the process of continuous charging and discharging, the influence of the passivation anode surface with uneven ionic conductivity on Zn deposition will continue to be amplified, resulting in significant non-uniform electric field, crazy growth of Zn dendrite, and eventually short circuit and other problems that seriously shorten the life of ZIBs [14,15].

Different approaches have been developed to tackle these aforementioned problems, such as anode structure design [16–18], separator modification [19], and electrolyte engineering [20]. While the design of complex anode structure regulates the uniform Zn deposition, it is also likely to increase the degree of side reaction and reduce the physicochemical stability of the material due to the increase in specific surface area. Separator modification also typically comes with the risk of increased interface impedance and reduced battery volume energy density. Furthermore, a lot of work has been conducted on "salt-in-water" electrolytes, but the high concentration of electrolytes increases the cost and is not conducive to the commercial promotion of ZIBs. As a bridge combining the anode with the cathode, the characteristics of the electrolyte, such as ion transport rate, play a significant role in the performance of the battery [21]. Therefore, cost-effective and facile electrolyte engineering deserves attention and is expected to improve the performance of ZIBs [22]. Liang et al. constructed functionalized massive solvation modules with the aid of maltose additives to homogenize zinc deposition, prevent parasitic reactions, and inhibit the structural collapse of active materials [23]. Fan et al. optimized the performance of zinc-ion hybrid capacitors based on self-recovering electrostatic shielding and the co-storage mechanism of Mg^{2+} and Zn^{2+} by utilizing $MgSO_4$ as an effective additive [24]. Qian et al. added slightly soluble silver sulfate ($AgSO_4$) to the electrolyte as an additive and established a continuously compensated zincophilic site with the help of the slow-release effect brought by its dissolution equilibrium. Thus, they achieved the effect of continuous regulation of zinc ion flux and electric field distribution and realized the improvement of battery performance [25]. Cheng et al. studied the effect of supramolecular macrocyclic (cyclodextrin) as an electrolyte additive on the stability of the Zn anode. Cyclodextrin with a rich negative charge can be adsorbed on the electrode surface, helping Zn^{2+} desolvation with its hydrophobic cavity, adjusting the diffusion and deposition kinetics, and realizing high-rate plating/stripping of batteries [13]. Based on the issues of uneven dendrite growth and hydrogen evolution of the anode and the solution of vanadium pentoxide cathode, Geon−Hyoung An et al. studied that adding vanadium oxide sulfate ($VOSO_4$) to the electrolyte can improve the performance of the battery in one step by inhibiting vanadium dissolution and stabilizing Zn deposition by self-forming a passivation layer on the anode surface [26]. However, most electrolyte additives fail to effectively protect the Zn anode and optimize ZIB performance. Furthermore, issues of the toxicity and high cost of electrolyte additives still exist that have to be considered for practical application.

Herein, the low-cost, nontoxic, and environmentally friendly sodium citrate (SC) is utilized as a dual-functional electrolyte additive in the 2 M $ZnSO_4$ (ZSO) electrolyte (Figure 1). As mentioned above, there are many problems on the surface of the Zn anode. When zinc ions formed solvated structures reach the surface of the zinc negative electrode,

the desolvation process occurs first, and then electronic behavior occurs. The active water generated via the desolvation process will decompose into H^+ and OH^- on the surface of the Zn anode, leading to severe hydrogen evolution and corrosion reactions. In the process of continuous charge and discharge cycle, a large number of ZHS, dead zinc, and zinc dendrites are formed, resulting in permanent failure of the ZIBs (Figure 1a). Surprisingly, the SC additive will alter the structure of $[Zn(H_2O)_6]^{2+}$ to form another style solvation shell, which contributes to the desolvation and inhibits side reactions. Additionally, the abundant sodium ions (Na^+) in SC with a lower effective reduction potential can form an electrostatic shield inhibiting the formation of initial surface bulges and subsequent Zn dendrites, making the electric field well-distributed at the anode interface and assisting stable 3D diffusion (Figure 1b). Accordingly, the dual-functional SC electrolyte additive effectively reduces the formation of dendrites and inhibits the production of byproducts. The Zn//Zn symmetric cell with 1 mM SC additive can be cycled at 1 and 5 mA cm^{-2} for about 760 h and 830 h, respectively. The Zn//Cu asymmetric cell can also stably operate at 1 mA cm^{-2} for 514 cycles with an average coulombic efficiency (CE) of 97.7%. A higher capacity retention of Zn//NVO cell (40.0%) after 400 cycles at 1 A g^{-1} is also realized compared with that of ZSO electrolyte (23.8%), which admirably demonstrates the practicability and effectiveness of the low-cost SC additive to assist ZIB applications in the future.

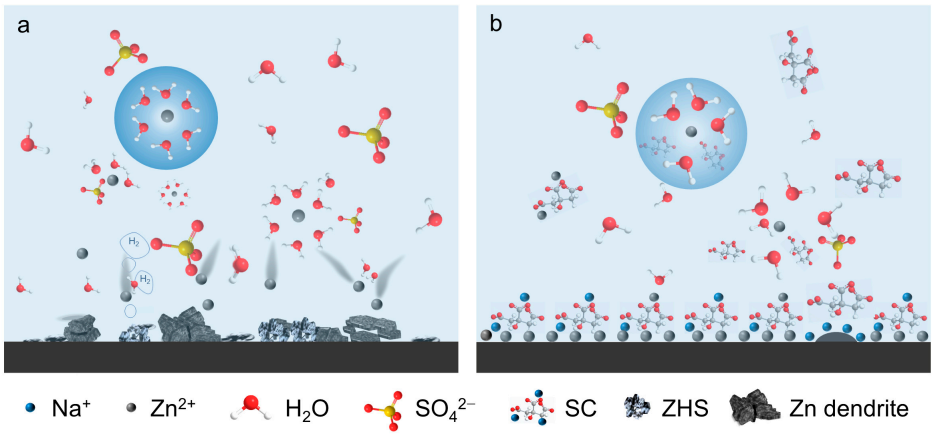

Figure 1. Schematics illustration of electrochemical behaviors at the anode/electrolyte interface in different electrolyte systems: (**a**) pure $ZnSO_4$ electrolyte and (**b**) $ZnSO_4$ electrolyte containing sodium citrate additive.

2. Materials and Methods

Materials: Vanadium pentoxide (V_2O_5, AR) was provided by Macklin. Zinc sulfate heptahydrate ($ZnSO_4 \cdot 7H_2O$, AR), SC, sodium chloride (NaCl, AR), and N-Methyl-2-pyrrolidone (NMP, >99.5%) were provided by Aladdin. All the chemicals were used without further purification.

Electrolyte preparation: A 2 M ZSO electrolyte was prepared with 3.45 g of $ZnSO_4 \cdot 7H_2O$ dissolved in 6 mL deionized water. A series of electrolytes containing SC additive with different concentrations (0.5, 1.0, 5.0, 10.0, and 30.0 mM) were prepared by adding different amounts (0.774 mg, 1.55 mg, 7.74 mg, 15.48 mg, and 46.45 mg) of SC to 6 mL of ZSO electrolyte (2 M). These solutions are denoted as ZSO-*x* SC (*x* represents concentration, ZSO-0.5 SC, ZSO-1.0 SC, ZSO-5.0 SC, ZSO-10.0 SC, and ZSO-30.0 SC, respectively).

NVO cathode preparation: The synthesis of NVO is referred to in the classical literature [27]. First, 2 g of commercial V_2O_5 powder was dissolved in 2 M NaCl solution (30 mL) and stirred for 96 h at room temperature. After repeated centrifugation and washing with deionized water, NVO powder was obtained after being dried in a freeze-dryer for 72 h. The resulting slurry was obtained by mixing synthesized NVO, carbon black, and polyvinylidene difluoride (PVDF) in a mass ratio of 7:2:1, which was coated on stainless

steel meshes and dried at 80 °C through vacuum drying overnight, followed by cutting into ϕ10 mm discs as NVO cathode.

Electrochemical measurements: The electrochemical performance, such as the long cycling and rate performance of the battery in this work, was measured using a battery testing system (Land CT3001A) in coin cells (CR-2032). The Zn//Zn symmetric cell, Zn//Cu asymmetrical battery, and Zn//NVO full cell were assembled using Zn foils as anode, Cu foils or NVO foils as cathode (ϕ10 mm), and glass fiber as a separator, with the addition of 100 μL of electrolyte (2 M ZSO or 2 M ZSO-*x* SC). The cut-off voltage of the Zn//Cu asymmetrical battery is 0.5 V. The charge and discharge cut-off voltage of the Zn//NVO full battery is 1.6V and 0.4V, respectively. Cyclic voltammetry (CV), chronoamperometry (CA), electrochemical impedance spectra (EIS), and Tafel test were conducted on the CHI-660E electrochemical workstation, with the frequency range of EIS from 0.01 Hz to 100 kHz, and the scanning rate of the CV and Tafel tests were fixed at 3 mV s^{-1} and 1 mV s^{-1}, respectively. Tafel curves were measured in a three-electrode system with Zn foil as the working electrode, Pt as the counter electrode, and Ag/AgCl as the reference electrode.

Material characterization: Scanning electron microscopy (SEM, Zeiss Supra 40 field-emission scanning electron microscope with an acceleration voltage of 5 kV, secondary electron image) was used to obtain images of the microstructure of zinc foil. Raman spectroscopy was collected on a Laser Confocal Raman Microscope (LabRAM HR Evolution) at a 532 nm wavelength. ^{1}H Nuclear magnetic resonance spectrum (^{1}H NMR, 400 MHz) was carried out on a Bruker AVANCE III 400, and DMSO-d6 was used for locking and shimming. X-ray diffraction (XRD) was recorded using the RigakuSmartLab X-ray diffractometer fitted with Cu-Kα X-ray (λ = 1.54 Å) radiation to gather structural and phase characterizations of the Zn foils.

3. Results and Discussion

3.1. Properties and Mechanism of Electrolyte with SC Additive

SC is an organic compound with a strong metal ion complexation ability and safe, non-toxic properties (Figure 2a) [28]. To understand the regulation mechanism of the SC additive on the solvation structure of Zn^{2+} in the electrolyte, Raman tests were carried out on the electrolyte containing different concentrations of SC additive (Figure 2b). Particularly, Raman spectra of v-SO_4^{2-} and v-(O−H) bands are analyzed as shown in Figure 2c,d. As the concentration of SC improves to 30 mM, the v-SO_4^{2-} band shifts to a lower wavenumber, implying that the association between Zn^{2+} and SO_4^{2-} has been weakened via the strong interaction between Zn^{2+} and SC (Figure 2c) [29]. Within the region from 2800 to 3800 cm^{-1} about the v-(O−H) band, the low-frequency region corresponds to the strong hydrogen bond, and the high-frequency region corresponds to the weak hydrogen bond [30]. When the SC content is increased, the peak area increases at low frequency, while at high frequency, the peak area decreases (Figure 2d). It indicates that the ratio of strong hydrogen bonds with lower bond energy increases, and the SC additive interacts with water by forming additional strong hydrogen bonds, resulting in the reduced content of free water in the electrolyte, which is conducive to reducing the occurrence of side reactions. Furthermore, compared with 2 M ZSO electrolyte, ^{1}H NMR displays the ^{1}H peak shifting from 4.009 ppm to 4.024 ppm when adding 1 mM SC additive in 2 M ZSO electrolyte (Figure 2e) [31]. This is because of the formation of hydrogen bonds with low diamagnetic shielding so that the resonance occurs down-field, indicating that adding a small amount of SC would produce hydrogen bonds with water, which may affect the solvated shell of Zn^{2+}. When the SC concentration increases to 10 and 30 mM, the chemical shift moves to the upfield compared to 1 mM, which may be caused by the pH change of the solution. Owing to the occurrence of sodium citrate containing massive hydrogen bond donors and acceptors, the solvation structure of Zn^{2+} is optimized, which contributes to the Zn^{2+} desolvation and reduces the occurrence of interface corrosion reactions. Additionally, the effective reduction potentials

of Zn^{2+} and Na^{+} are calculated according to the Nernst equation (Equation (1)) and listed in Table 1 [24]:

$$E_{Red} = E^{\theta}_{Red} - \frac{RT}{zF} \ln \frac{\alpha_{Red}}{\alpha_{Ox}}, \quad (1)$$

where E_{Red} is the effective reduction potential and reflects the ability to gain and lose electrons of the substances that make up the electrode, which is mainly affected by the standard reduction potential and the chemical activity for the relevant species; E^{θ}_{Red} is the standard reduction potential; R is the universal gas constant (8.314472 J K^{-1} mol^{-1}); T is the absolute temperature (T = 298.15 K); α is the chemical activity for the relevant species (α_{Red} is for the reductant and α_{Ox} for the oxidant); z is the number of electrons transferred; F is the Faraday constant (96,485.3399 C mol^{-1}). Because a large number of sodium ions with usually lower effective reduction potential at the appropriate concentrations in this experiment gather on the surface of the Zn anode to form an electrostatic shielding layer, the process of Zn deposition is affected, which can be observed through nucleation overpotential (NOP). According to the corresponding Equation (2):

$$r_{\text{crit}} = 2\frac{\gamma V_m}{F \cdot |\eta|}, \quad (2)$$

where γ is the surface energy of the anode/electrolyte interface, V_m is the molar volume of Zn, F and η are Faraday's constant and NOP; it can be induced that the smaller the nucleation overpotential, the larger the nucleation radius [15]. Figure 2f shows the NOP obtained via eletrodeposition of Zn//Cu asymmetric cells with different electrolyte systems at a current density of 1 mA cm^{-2}, in which the NOP of ZSO electrolyte is 18 mV increases to 20 mV after adding 0.5 mM SC, and the NOP raises significantly with the augment of concentration (10 mM corresponds to 61 mV). Similarly, with the increase in the concentration of SC additive, the concentration of Na^{+} enriched on the surface of the Zn anode increases, and the obstruction to Zn^{2+} deposition increases, resulting in the increase in NOP. The higher NOP with the introduction of SC indicates the denser Zn deposition and the smaller degree of side reactions.

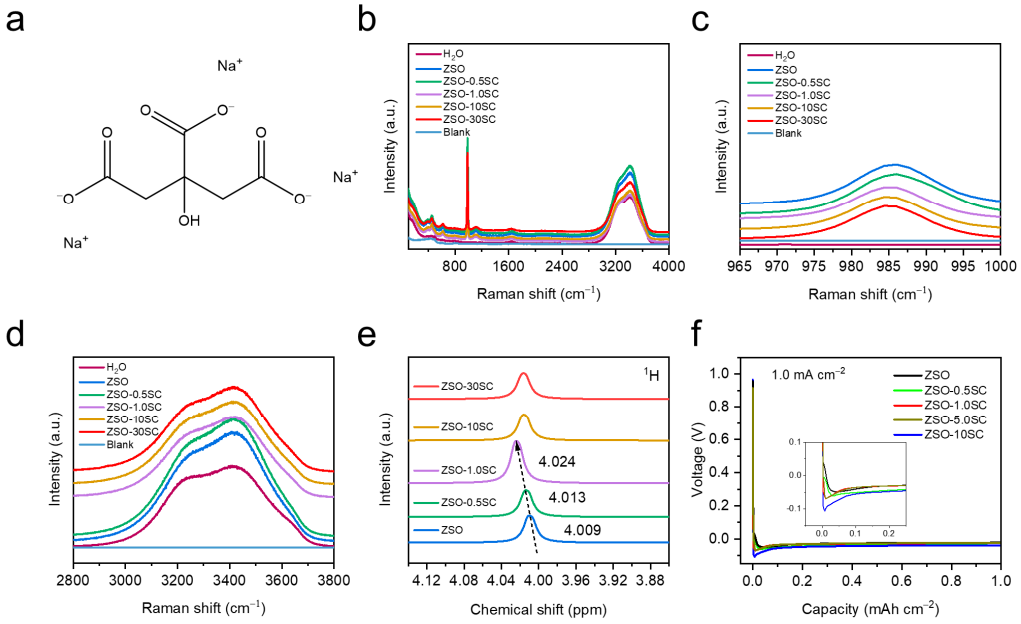

Figure 2. (**a**) Molecular formula of SC additive. (**b**) Raman spectra of H_2O, ZSO, and ZSO-x SC electrolyte. Raman spectra for (**c**) (v-SO_4^{2-}) and (**d**) (v-O–H) of ZSO electrolyte with/without various SC concentrations. (**e**) ^{1}H NMR spectra of ZSO electrolytes with/without various SC concentrations. (**f**) Nucleation overpotential of Zn//Cu asymmetric cells with different electrolytes.

Table 1. Effective reduction potentials of Na^+ and Zn^{2+} (vs. SHE) at the appropriate concentrations correspond to different electrolytes (2 M ZSO, 2M-0.5 SC, 2M-1.0 SC, 2M-5.0 SC, and 2M-10 SC) in this study.

Cation	E^{θ}_{Red}	Effective Reduction Potential (E_{Red},V)				
	1.0 M	**1.5 mM**	**3.0 mM**	**15 mM**	**30 mM**	**2.0 M**
Zn^{2+}	−0.762	−0.846	−0.837	−0.816	−0.807	−0.753
Na^+	−2.71	−2.877	−2.859	−2.818	−2.800	−2.692

Ion migration and transport difficulty are essential arguments to investigate the effectiveness of electrolyte additives. Accordingly, ion conductivity (σ) and ion transference number (t_B, B represents ion) of different electrolyte systems are analyzed and presented in Figure 3a–g [30]. Ion conductivity is determined in accordance with the EIS of SS//SS symmetric cells (Figure 3a) and the corresponding Equation (3):

$$\sigma = \frac{l}{R \cdot A}, \tag{3}$$

where l is the thickness of the electrolyte, R is the bulk resistance, and A is the contact area of the electrolyte [32]. It is surprising to find that the 2 M ZSO-x SC electrolyte exhibits a higher ionic conductivity than the 2 M ZSO electrolyte, as shown in Table 2. This may be the result of the SC additive affecting the solvation structure of Zn^{2+} and increasing the rate of ion transport. Meanwhile, the Zn^{2+} transfer number ($t_{Zn^{2+}}$) measures the ability of the electrolyte to transport cations instead of anions, thereby alleviating the concentration gradient caused by Zn deposition at the anode surface and accelerating reaction kinetics. This can be calculated using Equation (4):

$$t_{Zn^{2+}} = \frac{I_s(\Delta V - R_0 I_0)}{I_0(\Delta V - R_s I_s)}, \tag{4}$$

where ΔV is the applied polarization potential (ΔV = 25 mV, 600 s); I_0 and I_s are the initial and steady-state currents, respectively; R_0 and R_s represent initial-state impedances and steady-state impedances, respectively [33]. As shown in Figure 3b, the I_0 and I_s after potentiostatic polarization for 600 s using 2 M ZSO-1.0 SC electrolyte are 0.067 mA and 0.035 mA, respectively, similar to those without SC additive (0.0465 mA and 0.0235 mA). After constant potentiostatic polarization, concentration polarization occurs at the anode–electrolyte interface, resulting in increased internal resistance of the battery, and R_s is higher than R_0 [34]. However, compared with pure 2 M ZSO electrolyte, the R_0 and R_s of Zn symmetric batteries with 2 M ZSO-1.0 SC electrolyte before and after potentiostatic polarization are much smaller (before 280 Ω vs. 410 Ω, after 590 Ω vs. 720 Ω, respectively, Figure 3c,d). At last, the $t_{Zn^{2+}}$ of 2 M ZSO-1.0 SC is calculated to be 0.75, which is significantly increased compared with 2 M ZSO electrolyte (0.38), further demonstrating that the SC additive promotes the Zn^{2+} desolvation by effectively inhibiting the migration of SO_4^{2-} anions. The nucleation and growth behavior on the Zn anode can also be revealed by observing the current–time curves through CA testing under overpotential conditions (−200 mV). As shown in Figure 2e, in the initial state, when the current drops sharply with time, a two-dimensional (2D) diffusion process dominates on the Zn surface. Subsequently, the current gradually stabilizes into the stage of 3D diffusion in ZSO-1.0 SC, while the current continues to increase in ZSO, which represents a longer 2D diffusion and a higher probability of Zn dendrite growth [35]. Furthermore, Tafel curves were conducted to compare the corrosion current between the two types of electrolytes via monitoring the linear polarization tests, as shown in Figure 3f. The addition of SC offers a smaller corrosion current density (1.669 mA cm^{-2}) than that of pure 2 M ZSO electrolyte (2.888 mA cm^{-2}), indicating less tendency of corrosion for Zn foil in ZSO electrolyte with SC additive [36]. As shown in SEM and XRD results (Figure 3g–i), this conclusion was also verified by soaking Zn foil in

different electrolytes for 5 days. The surface topography of Zn foil soaked in 2 M ZSO-1.0 SC after 5 days only shows a small amount of flakes. Without SC additive, a large amount of zinc dendrites and flakes are observed, with the formation of zinc hydroxyl sulfate particles as evidenced by the XRD peaks centered at 9.5°, 18.6°, and 26.2° ($(Zn(OH)_2)_3(ZnSO_4)\cdot(H_2O)_3$, PDF#78-0247).

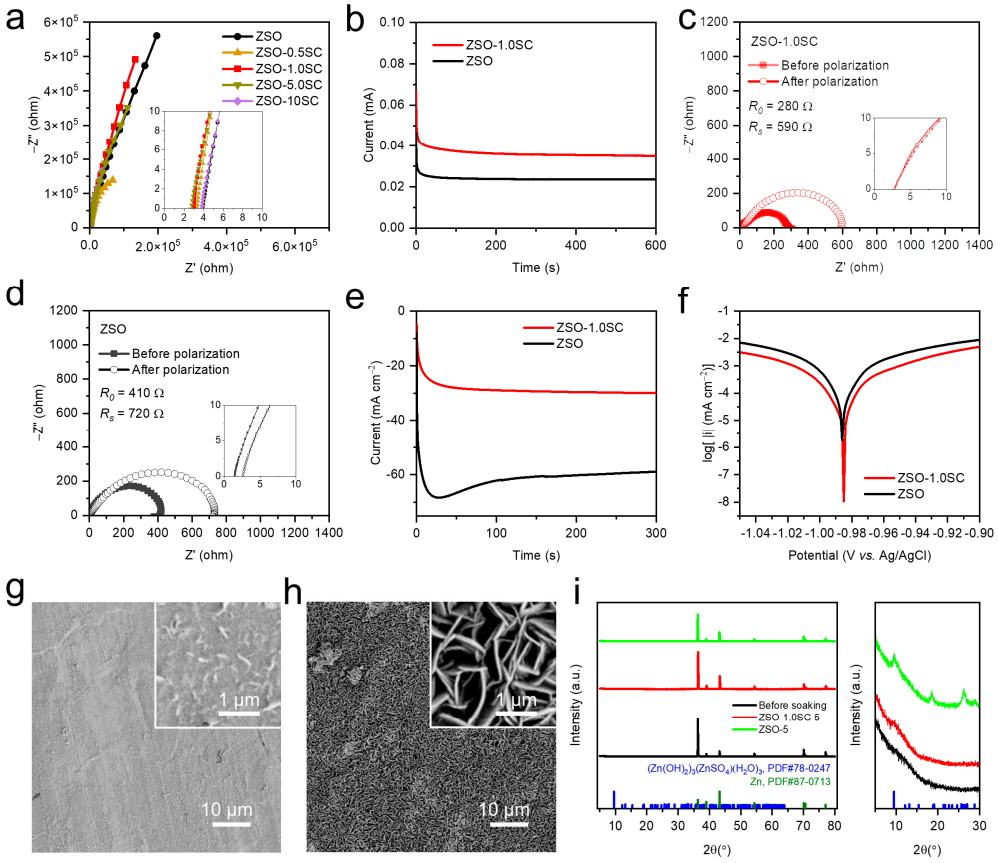

Figure 3. (**a**) Nyquist plots of stainless steel (SS) symmetrical cells with different electrolytes. (**b**) CA test of Zn symmetrical cell using 2 M ZSO-1.0 SC electrolyte and 2 M ZSO electrolyte. Corresponding AC impedance spectra before and after CA test: (**c**) with and (**d**) without SC additive. (**e**) CA of Zn//Zn symmetric cells with/without SC additive at a −200 mV overpotential. (**f**) Linear polarization curves with different electrolytes. SEM images of Zn foil after soaking in the (**g**) 2 M ZSO-1.0 SC electrolyte and (**h**) 2 M ZSO electrolyte for 5 days. (**i**) Corresponding XRD patterns of Zn foil after soaking for 5 days.

Table 2. Ionic conductivity of different electrolytes.

Sample	Thickness	R_0	Area	Ionic Conductivity
	μm	Ω	cm^{-2}	mS cm^{-1}
ZSO-0.5 SC	276	3.3	0.785	10.65
ZSO-1.0 SC	276	3.1	0.785	11.34
ZSO-5.0 SC	276	2.8	0.785	12.56
ZSO-10 SC	276	3.9	0.785	9.02
ZSO	276	4.2	0.785	8.37

3.2. Electrochemical Properties of Electrolytes with SC Additive

In consideration of the electrostatic shielding effect of SC on the Zn anode, the deposition process should be further analyzed [37]. CV curves of the Zn//Cu asymmetrical batteries with different electrolytes are measured to expose Zn nucleation processes (Figure 4a). Certainly, the NOP of Cu//Zn with 2 M ZSO-1.0 SC electrolyte is 83.0 mV,

higher than that of the Cu//Zn with 2 M ZSO electrolyte (62.7 mV), consistent with the previous result shown in Figure 2e. As a key parameter to evaluate Zn plating/stripping reversibility, the CE of the Zn//Cu asymmetrical battery is tested under 1 mA cm^{-2} with a cut-off voltage of 0.5 V [29]. As shown in Figure 4b, the Zn//Cu battery with SC additive manifests stable Zn deposition/dissolution with an average CE of 97.7% after 514 cycles. However, for the Zn//Cu battery without SC additive, the CE changes violently only after 170 cycles. Comparing the corresponding voltage profiles of Zn//Cu asymmetrical cells and CV curves (Figure 4a,c,d), it can be proven that adding SC additive does not change the original oxidation and reduction process of the battery. Meanwhile, the Zn//Zn symmetric cell with SC additive also presents a longer cycle time (760 h) with a smaller voltage fluctuation (37 mV) than the Zn symmetric cell without SC additive (117 h and 53 mV, Figure 4e). Additionally, the corresponding Zn anodes in the symmetric cell after 50 cycles are investigated through SEM and XRD. The surface morphology of the Zn anode with SC additive remains flat and dense, in contrast to the plentiful dendrites and byproducts on the Zn anode cycled in symmetric cells without SC additive (Figure 4f–g). The XRD results in Figure 4h reveal that these byproducts are $(Zn(OH)_2)_3$ $(ZnSO_4)\cdot(H_2O)_3$ (PDF#78-0247), while no characteristic byproduct peaks are observed on Zn foil cycled in symmetric cells with SC additive. These results demonstrate that dual-functional SC, providing hydrogen-bond donors and hydrogen-bond acceptors, can optimize ZIB performance by adjusting the solvation structure, accelerating the Zn^{2+} desolvation, while the electrostatic shielding effect of Na^+ homogenizes the interfacial electric field distribution [38–40]. The rate performance test of symmetrical batteries assembled with different electrolytes can be used to detect the anode interface. As shown in Figure 4i, although the two symmetric cells exhibit similar polarization voltages in the change of current density from 0.5 mA cm^{-2} to 10 mA cm^{-2}, the cell without SC additive suffers a short circuit in the change of current density from 10 mA cm^{-2} to 0.5 mA cm^{-2}, which means more serious dendrite growth and side reactions inside. To further verify the effect of SC concentrations for electrochemical properties on the Zn anode, symmetrical batteries were assembled, and the galvanostatic cycling performance was tested (Figure 4j). The results show that the cycle life varies greatly (only 37 h with ZSO electrolyte, 54 h with 0.5 mM SC, 830 h with 1.0 mM SC, 421 h with 5.0 mM SC, and 328 h with 10.0 mM SC). When the concentration of SC additive increases to a certain extent, the battery cycle life increases. But when too high, it would have a negative impact on the performance of the battery. Related to nucleation overpotential (Figure 2f), the high concentration of Na^+ on the surface of the Zn anode may lead to more difficult Zn deposition and a more serious tip discharge effect, which results in the failure of the battery due to a short circuit.

To demonstrate the feasibility of SC electrolyte additives for ZIBs, assembled Zn//NVO full batteries were measured by matching NVO cathode, which exhibits the special nanobelt structure and an H^+ and Zn^{2+} insertion/extraction mechanism simultaneously with a theoretical specific capacity (380 mAh g^{-1}) [27,41]. Obviously, with 1 mM SC additive as the object of this study, the overall performance of the Zn//NVO full cell is effectively improved compared to that without SC, as shown in CV, EIS, and rate performance (Figure 5a–c). The CV curves of the full cell with SC additive in Figure 5a show slightly higher current density between the reduction and oxidation peaks than that with pure ZSO electrolyte, which may be ascribed to SC that contributes to the insertion process and inhibits the occurrence of side reactions (Figure 5a), consistent with EIS measurement of a smaller charge transfer resistance (Figure 5b) [42]. Compared with the 2 M ZSO electrolyte, the rate performance of the Zn//NVO battery with SC additive also exhibits a more enhanced specific capacity at different current densities, changing from 0.1 A g^{-1} to 5 A g^{-1} and back to 0.1 A g^{-1} in Figure 5c, indicating the accelerated reaction rate [36,43]. Clearly, with the assistance of SC additive, the performance of the Zn//NVO full battery is slightly optimized at 1 A g^{-1} (a higher capacity of 100.8 mAh g^{-1} with a capacity retention rate of 40.0% after 400 cycles), while the capacity of that with pure ZSO electrolyte sharply drops to 63.6 mAh g^{-1} with a lower capacity retention rate of 23.8% (Figure 5d–f). Furthermore,

it can also be demonstrated that the Zn//NVO full cell using 2 M ZSO-1.0 SC electrolyte delivers a higher CE of 72.92%, which is much better than that without SC additive (64.21%) when monitoring the open-circuit voltage drop after 48 h rest (Figure 5g). As mentioned above, SC electrolyte additives improve the electrochemical properties of batteries by accelerating the desolvation process of zinc ions and uniform Zn deposition, which significantly homogenizes the electric field distribution and inhibits Zn dendrite formation and side reactions.

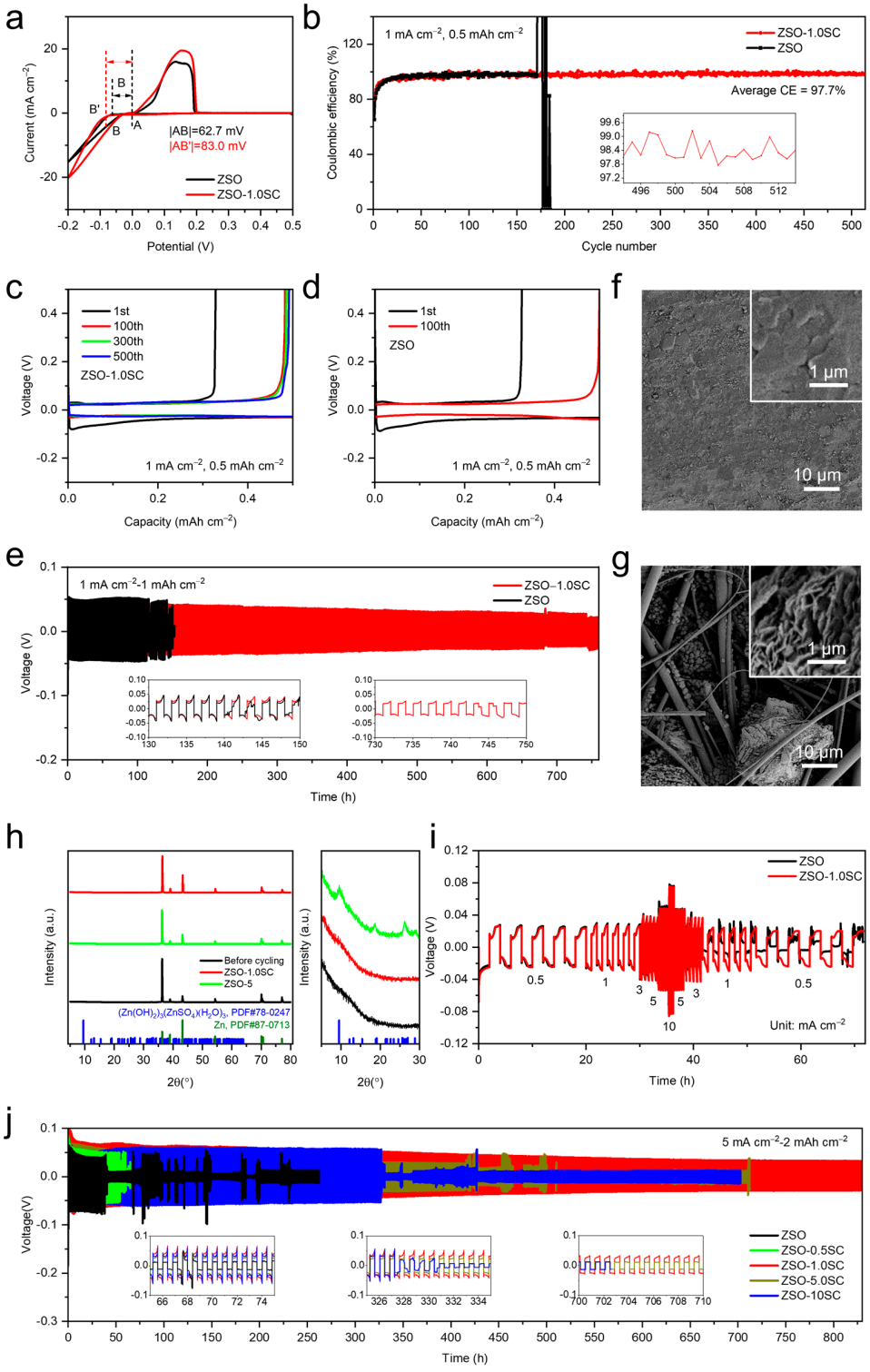

Figure 4. (**a**) CV curves for Zn nucleation on Cu foil with/without SC additive. (**b**) CE and (**c**) and (**d**) the corresponding voltage profiles of Zn//Cu asymmetrical cells at 1.0 mA cm^{-2} with/without

SC additive. (**e**) Long-term cycling stability, (**f**,**g**) the corresponding SEM picture and (**h**) XRD patterns of Zn foil obtained from Zn symmetrical cells after 50 cycles with ZSO electrolyte or ZSO-1.0 SC electrolyte at 1.0 mA cm^{-2}. (**i**) Rate performance of Zn symmetrical cells at different current densities from 0.5 mA cm^{-2} to 10 mA cm^{-2} and a fixed charge/discharge capacity of 1 mA h cm^{-2}. (**j**) Cycling performance of Zn//Zn symmetric cells at 5 mA cm^{-2}.

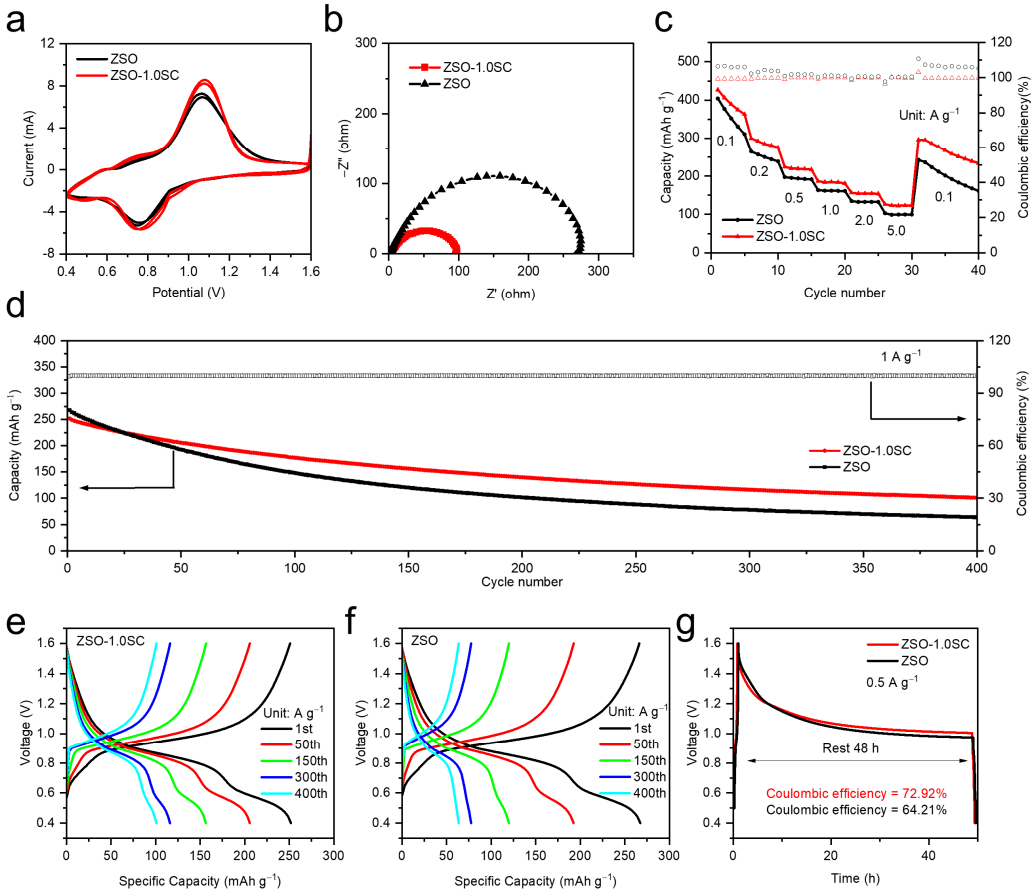

Figure 5. (**a**) CV curves, (**b**) EIS, and (**c**) rate performance of a Zn//NVO full cell using ZSO with SC electrolyte or pure ZSO electrolyte. (**d**) Long-term cycling performance comparison. (**e**,**f**) Corresponding charge and discharge curves of the full cell with/without SC additive at 1 A g^{-1}. Self-discharging evaluation of Zn//NVO full cells using (**g**) ZSO with SC electrolyte and pure ZSO electrolyte after 48 h rest at 0.5 A g^{-1}.

4. Conclusions

With homogenized electric field distribution and facilitated Zn^{2+} desolvation, the electrochemical performance of ZIBs is effectively improved by utilizing SC as an electrolyte additive. Particularly, SC realizes rapid Zn^{2+} desolvation and Zn deposition kinetics by readjusting the solvation environment of Zn^{2+} and inhibiting side reactions. Furthermore, Na^{+} in SC exhibits a lower effective reduction potential than Zn^{2+}, resulting in a higher concentration of Na^{+} at the anode surface and the generation of an electrostatic shield layer, which assists with homogenizing the electric field distribution and restraining Zn dendrite growth. Therefore, electrolyte with SC additive can greatly protect Zn anode from the growth of Zn dendrite, HER, and corrosion reactions, thus allowing durable Zn//Zn symmetric batteries with cycling stability of more than 760 h at 1 mA cm^{-2} and 830 h at 5 mA cm^{-2}, Zn//Cu asymmetric batteries with high CE (97.7%) at 1 mA cm^{-2}, and Zn//NVO full cells with a stable high capacity (100.8 mAh g^{-1}) after 400 cycles at 1 A g^{-1}. It is envisioned that this study could provide valuable insight into seeking electrolyte additive to develop environmentally friendly, practical, and durable ZIBs.

Author Contributions: X.L. designed the experiment. X.L., L.Y., W.D. and Y.Q. performed experimental procedures, investigation of materials, software programming to process and collect data, data analysis, and wrote the manuscript. All authors reviewed the manuscript. All authors have read and agreed to the published version of the manuscript.

Funding: This research was funded by the USTC Startup Program (KY2090000062, KY2090000098, KY2090000099).

Institutional Review Board Statement: Not applicable.

Informed Consent Statement: Not applicable.

Data Availability Statement: The data that support the findings of this study are available from the authors upon reasonable request.

Acknowledgments: This work was financially supported by the USTC Startup Program (KY2090000062, KY2090000098, KY2090000099) and the Joint Research Center for Multi-Energy Complementation and Conversion. The data were partially carried out at the USTC Center for Micro and Nanoscale Research and Fabrication.

Conflicts of Interest: The authors declare no conflicts of interest.

References

1. Li, G.; Zhao, Z.; Zhang, S.; Sun, L.; Li, M.; Yuwono, J.A.; Mao, J.; Hao, J.; Vongsvivut, J.; Xing, L.; et al. A biocompatible electrolyte enables highly reversible Zn anode for zinc ion battery. *Nat. Commun.* **2023**, *14*, 6526. [CrossRef]
2. Yang, C.; Wu, Q.; Xie, W.; Zhang, X.; Brozena, A.; Zheng, J.; Garaga, M.N.; Ko, B.H.; Mao, Y.; He, S.; et al. Copper-coordinated cellulose ion conductors for solid-state batteries. *Nature* **2021**, *598*, 590–596. [CrossRef] [PubMed]
3. Meng, Y.S.; Srinivasan, V.; Xu, K. Designing better electrolytes. *Science* **2022**, *378*, eabq3750. [CrossRef] [PubMed]
4. Kim, M.S.; Ryu, J.-H.; Deepika; Lim, Y.R.; Nah, I.W.; Lee, K.-R.; Archer, L.A.; Il Cho, W. Langmuir–Blodgett artificial solid-electrolyte interphases for practical lithium metal batteries. *Nat. Energy* **2018**, *3*, 889–898. [CrossRef]
5. Bruce, P.G.; Freunberger, S.A.; Hardwick, L.J.; Tarascon, J.-M. Li–O_2 and Li–S batteries with high energy storage. *Nat. Mater.* **2012**, *11*, 19–29. [CrossRef]
6. Wang, F.; Borodin, O.; Gao, T.; Fan, X.; Sun, W.; Han, F.; Faraone, A.; Dura, J.A.; Xu, K.; Wang, C. Highly reversible zinc metal anode for aqueous batteries. *Nat. Mater.* **2018**, *17*, 543–549. [CrossRef]
7. Zheng, J.; Zhao, Q.; Tang, T.; Yin, J.; Quilty, C.D.; Renderos, G.D.; Liu, X.; Deng, Y.; Wang, L.; Bock, D.C.; et al. Reversible epitaxial electrodeposition of metals in battery anodes. *Science* **2019**, *366*, 645–648. [CrossRef]
8. Liu, A.N.; Wu, F.; Zhang, Y.X.; Jiang, Y.; Xie, C.; Yang, K.Q.; Zhou, J.H.; Xie, M. Ultralarge layer spacing and superior structural stability of V_2O_5 as high-performance cathode for aqueous zinc-ion battery. *Nano Res.* **2023**, *16*, 9461–9470. [CrossRef]
9. Sun, G.Q.; Zhou, M.Q.; Dong, X.Y.; Zang, S.Q.; Qu, L.T. An efficient and versatile biopolishing strategy to construct high performance zinc anode. *Nano Res.* **2022**, *15*, 5081–5088. [CrossRef]
10. Xia, X.Y.; Zhao, Y.J.; Zhao, Y.; Xu, M.G.; Liu, W.; Sun, X.M. Mo doping provokes two electron reaction in MnO_2 with ultrahigh capacity for aqueous zinc ion batteries. *Nano Res.* **2023**, *16*, 2511–2518. [CrossRef]
11. Sun, W.; Wang, F.; Hou, S.; Yang, C.; Fan, X.; Ma, Z.; Gao, T.; Han, F.; Hu, R.; Zhu, M.; et al. Zn/MnO_2 Battery Chemistry with H^+ and Zn^{2+} Coinsertion. *J. Am. Chem. Soc.* **2017**, *139*, 9775–9778. [CrossRef]
12. Zhang, N.; Cheng, F.; Liu, Y.; Zhao, Q.; Lei, K.; Chen, C.; Liu, X.; Chen, J. Cation-Deficient Spinel $ZnMn_2O_4$ Cathode in $Zn(CF_3SO_3)_2$ Electrolyte for Rechargeable Aqueous Zn-Ion Battery. *J. Am. Chem. Soc.* **2016**, *138*, 12894–12901. [CrossRef] [PubMed]
13. Zhao, K.; Fan, G.; Liu, J.; Liu, F.; Li, J.; Zhou, X.; Ni, Y.; Yu, M.; Zhang, Y.-M.; Su, H.; et al. Boosting the Kinetics and Stability of Zn Anodes in Aqueous Electrolytes with Supramolecular Cyclodextrin Additives. *J. Am. Chem. Soc.* **2022**, *144*, 11129–11137. [CrossRef] [PubMed]
14. Feng, D.; Jiao, Y.; Wu, P. Guiding Zn Uniform Deposition with Polymer Additives for Long-lasting and Highly Utilized Zn Metal Anodes. *Angew. Chem. Int. Ed.* **2023**, *62*, e202314456. [CrossRef] [PubMed]
15. Zhao, Z.; Zhao, J.; Hu, Z.; Li, J.; Li, J.; Zhang, Y.; Wang, C.; Cui, G. Long-life and deeply rechargeable aqueous Zn anodes enabled by a multifunctional brightener-inspired interphase. *Energy Environ. Sci.* **2019**, *12*, 1938–1949. [CrossRef]
16. Zeng, L.; He, H.; Chen, H.; Luo, D.; He, J.; Zhang, C. 3D Printing Architecting Reservoir-Integrated Anode for Dendrite-Free, Safe, and Durable Zn Batteries. *Adv. Energy Mater.* **2022**, *12*, 2103708. [CrossRef]
17. Xue, P.; Guo, C.; Li, L.; Li, H.; Luo, D.; Tan, L.; Chen, Z. A MOF-Derivative Decorated Hierarchical Porous Host Enabling Ultrahigh Rates and Superior Long-Term Cycling of Dendrite-Free Zn Metal Anodes. *Adv. Mater.* **2022**, *34*, 2110047. [CrossRef] [PubMed]
18. Joseph, F.; Parker; Chervin, C.N.; Pala, I.R.; Machler, M.; Burz, M.F.; Long, J.W.; Rolison, D.R. Rechargeable nickel–3D zinc batteries: An energy-dense, safer alternative to lithium-ion. *Science* **2017**, *356*, 415–418.

19. Zhao, N.; Liang, Y.; Huo, W.; Zhu, X.; He, Z.; Zhang, Z.; Zhang, Y.; Wu, X.; Dai, L.; Zhu, J.; et al. Separator functionalization enables high-performance zinc anode via ion-migration regulation and interfacial engineering. *Chin. Chem. Lett.* **2023**, 109332. [CrossRef]
20. Shao, W.; Li, C.; Wang, C.; Du, G.; Zhao, S.; Qu, G.; Xing, Y.; Guo, T.; Li, H.; Xu, X. Stabilization of zinc anode by trace organic corrosion inhibitors for long lifespan. *Chin. Chem. Lett.* **2024**, 109531. [CrossRef]
21. Hao, J.; Long, J.; Li, B.; Li, X.; Zhang, S.; Yang, F.; Zeng, X.; Yang, Z.; Pang, W.K.; Guo, Z. Toward High-Performance Hybrid Zn-Based Batteries via Deeply Understanding Their Mechanism and Using Electrolyte Additive. *Adv. Funct. Mater.* **2019**, *29*, 1903605. [CrossRef]
22. Guo, X.; Zhang, Z.; Li, J.; Luo, N.; Chai, G.-L.; Miller, T.S.; Lai, F.; Shearing, P.; Brett, D.J.L.; Han, D.; et al. Alleviation of Dendrite Formation on Zinc Anodes via Electrolyte Additives. *ACS Energy Lett.* **2021**, *6*, 395–403. [CrossRef]
23. Chen, W.; Guo, S.; Qin, L.; Li, L.; Cao, X.; Zhou, J.; Luo, Z.; Fang, G.; Liang, S. Hydrogen Bond-Functionalized Massive Solvation Modules Stabilizing Bilateral Interfaces. *Adv. Funct. Mater.* **2022**, *32*, 2112609. [CrossRef]
24. Wang, P.; Xie, X.; Xing, Z.; Chen, X.; Fang, G.; Lu, B.; Zhou, J.; Liang, S.; Fan, H.J. Mechanistic Insights of Mg^{2+}-Electrolyte Additive for High-Energy and Long-Life Zinc-Ion Hybrid Capacitors. *Adv. Energy Mater.* **2021**, *11*, 2101158. [CrossRef]
25. Zeng, X.; Qian, S.; Zhou, J.; Hao, B.; Zhang, L.; Zhou, Y.; Shi, Y.; Zhu, C.; Zhou, X.; Liu, J.; et al. Sustained-Compensated Interfacial Zincophilic Sites to Assist High-Capacity Aqueous Zn Metal Batteries. *Nano Lett.* **2023**, *23*, 1135–1143. [CrossRef]
26. Yoo, G.; Lee, Y.-G.; Im, B.; Kim, D.G.; Jo, Y.-R.; An, G.H. Integrated solution for a stable and high-performance zinc-ion battery using an electrolyte additive. *Energy Storage Mater.* **2023**, *61*, 102845. [CrossRef]
27. Wan, F.; Zhang, L.; Dai, X.; Wang, X.; Niu, Z.; Chen, J. Aqueous rechargeable zinc/sodium vanadate batteries with enhanced performance from simultaneous insertion of dual carriers. *Nat. Commun.* **2018**, *9*, 1656. [CrossRef] [PubMed]
28. Zhang, R.; Tang, Z.; Sun, D.; Li, R.; Yang, W.; Zhou, S.; Xie, Z.; Tang, Y.; Wang, H. Sodium citrate as a self-sacrificial sodium compensation additive for sodium-ion batteries. *Chem. Commun.* **2021**, *57*, 4243–4246. [CrossRef]
29. Wang, B.; Zheng, R.; Yang, W.; Han, X.; Hou, C.; Zhang, Q.; Li, Y.; Li, K.; Wang, H. Synergistic Solvation and Interface Regulations of Eco-Friendly Silk Peptide Additive Enabling Stable Aqueous Zinc-Ion Batteries. *Adv. Funct. Mater.* **2022**, *32*, 2112693. [CrossRef]
30. Li, T.C.; Lim, Y.; Li, X.L.; Luo, S.; Lin, C.; Fang, D.; Xia, S.; Wang, Y.; Yang, H.Y. A Universal Additive Strategy to Reshape Electrolyte Solvation Structure toward Reversible Zn Storage. *Adv. Energy Mater.* **2022**, *12*, 2103231. [CrossRef]
31. Feng, D.; Cao, F.; Hou, L.; Li, T.; Jiao, Y.; Wu, P. Immunizing Aqueous Zn Batteries against Dendrite Formation and Side Reactions at Various Temperatures via Electrolyte Additives. *Small* **2021**, *17*, 2103195. [CrossRef]
32. Lee, C.-J.; Wu, H.; Hu, Y.; Young, M.; Wang, H.; Lynch, D.; Xu, F.; Cong, H.; Cheng, G. Ionic Conductivity of Polyelectrolyte Hydrogels. *Acs Appl. Mater. Inter.* **2018**, *10*, 5845–5852. [CrossRef]
33. Chu, Y.; Zhang, S.; Wu, S.; Hu, Z.; Cui, G.; Luo, J. In situ built interphase with high interface energy and fast kinetics for high performance Zn metal anodes. *Energy Environ. Sci.* **2021**, *14*, 3609–3620. [CrossRef]
34. Wang, J.; Zhu, Q.; Li, F.; Chen, J.; Yuan, H.; Li, Y.; Hu, P.; Kurbanov, M.S.; Wang, H. Low-temperature and high-rate Zn metal batteries enabled by mitigating Zn^{2+} concentration polarization. *Chem. Eng. J.* **2022**, *433*, 134589. [CrossRef]
35. Yang, H.; Qiao, Y.; Chang, Z.; Deng, H.; Zhu, X.; Zhu, R.; Xiong, Z.; He, P.; Zhou, H. Reducing Water Activity by Zeolite Molecular Sieve Membrane for Long-Life Rechargeable Zinc Battery. *Adv. Mater.* **2021**, *33*, 2102415. [CrossRef]
36. Chen, Y.; Gong, F.; Deng, W.; Zhang, H.; Wang, X. Dual-function electrolyte additive enabling simultaneous electrode interface and coordination environment regulation for zinc-ion batteries. *Energy Storage Mater.* **2023**, *58*, 20–29. [CrossRef]
37. Shangguan, M.; Wang, K.; Zhao, Y.; Xia, L. Tetraethylene Glycol Dimethyl Ether (TEGDME)-Water Hybrid Electrolytes Enable Excellent Cyclability in Aqueous Zn-Ion Batteries. *Batteries* **2023**, *9*, 462. [CrossRef]
38. Ding, F.; Xu, W.; Graff, G.L.; Zhang, J.; Sushko, M.L.; Chen, X.; Shao, Y.; Engelhard, M.H.; Nie, Z.; Xiao, J.; et al. Dendrite-Free Lithium Deposition via Self-Healing Electrostatic Shield Mechanism. *J. Am. Chem. Soc.* **2013**, *135*, 4450–4456. [CrossRef] [PubMed]
39. Geng, Y.; Pan, L.; Peng, Z.; Sun, Z.; Lin, H.; Mao, C.; Wang, L.; Dai, L.; Liu, H.; Pan, K.; et al. Electrolyte additive engineering for aqueous Zn ion batteries. *Energy Storage Mater.* **2022**, *51*, 733–755. [CrossRef]
40. Song, Y.; Zhang, K.; Li, X.; Yan, C.; Liu, Q.; Tang, A. Tuning the ferrous coordination structure enables a highly reversible Fe anode for long-life all-iron flow batteries. *J. Mater. Chem. A* **2021**, *9*, 26354–26361. [CrossRef]
41. Qiu, K.; Trudgeon, D.; Li, X.; Yufit, V.; Chakrabarti, B.; Brandon, N.; Shah, A. Study of Quaternary Ammonium Additives towards High-Rate Zinc Deposition and Dissolution Cycling for Application in Zinc-Based Rechargeable Batteries. *Batteries* **2022**, *8*, 106. [CrossRef]
42. Yu, H.; Chen, D.; Li, Q.; Yan, C.; Jiang, Z.; Zhou, L.; Wei, W.; Ma, J.; Ji, X.; Chen, Y.; et al. In Situ Construction of Anode–Molecule Interface via Lone-Pair Electrons in Trace Organic Molecules Additives to Achieve Stable Zinc Metal Anodes. *Adv. Energy Mater.* **2023**, *13*, 2300550. [CrossRef]
43. He, J.; Tang, Y.; Liu, G.; Li, H.; Ye, M.; Zhang, Y.; Yang, Q.; Liu, X.; Li, C. Intrinsic Hydrogen-Bond Donors-Lined Organophosphate Superionic Nanochannels Levering High-Rate-Endurable Aqueous Zn Batteries. *Adv. Energy Mater.* **2022**, *12*, 2202661. [CrossRef]